Journal of the Korean Physical Society, Vol. 47, August 2005, pp. S101∼S108

Waveguide Behavior of Distributed Bragg Reflectors Probed by Polarization-Modulated Near-Field Optical Microscopy

P. G. Gucciardi
CNR-Istituto per i Processi Chimico-Fisici, sez. Messina, Via La Farina 237, I-98123 Messina, Italy

M. Allegrini
INFM and Dipartimento di Fisica, Università di Pisa, Via Buonarroti 2, I-56126 Pisa, Italy

R. Micheletto,* T. Kotani, T. Hatada and Y. Kawakami
Department of Electronic Science, Graduate School of Engineering, Kyoto University, Nishikyo-ku, Katsura, 615-8510 Kyoto, Japan.

(Received 5 September 2004)

Distributed Bragg Reflectors (DBRs) have been found to be very effective in increasing the efficiency of light emitting diodes and semiconductor laser devices. By using polarization-modulated scanning near-field optical microscopy (PM-SNOM), we investigate the optical response to different illumination polarization states of a DBR structure that consists of a stack of quarter wavelength thick slabs of dielectrics with alternating high and low refractive index. The DBR has been optically characterized in the near-field at different wavelengths in illumination- and in collection- mode with light excitation orthogonal to the probe axis, for fixed as well as for modulated polarization. We have found that the optical signal does not follow the morphological structure of the slabs, as expected but it shows a different spatial periodicity related to the excitation properties and to the interplay of the different DBR planes.

PACS numbers: 07.79.Fc, 68.37.Uv, 95.75.Hi, 42.82.-m
Keywords: Scanning near-field optical microscopy, Distributed bragg reflectors, Polarization control

I. INTRODUCTION

Distributed Bragg Reflectors (DBRs) are gratings used in integrated laser technology to decrease standard mirror losses, resulting in a reduced lasing threshold and in a further shrinking of the device's dimension [1, 2]. It has been shown in fact that high reflectivity mirrors can be formed by deeply etching semiconductor/air DBRs, enhancing the optical feedback into the laser cavity [3, 4]. The implementation of DBR structures is particularly suited to increase the low facet reflectivity of InGaN/GaN lasers (∼18 %), due to the small refractive index of GaN-based materials (∼2.5). As a consequence, the operating current can be reduced to values comparable to those of GaAs/AlGaAs or GaInAsP/InP lasers [5, 6]. The characteristics of DBRs depend strongly on the geometrical structure of the grating. Several theoretical studies have been made to optimize the DBR design, maximizing the performance in edge-emitting lasers [1, 7,8]. From the experimental point of view, the efficiency of DBRs is studied by the direct implementation on a lasing device. On the other hand, Scanning Electron Microscopy (SEM) is the technique most widely used for the analysis of their morphology [5,6]. Scanning Near-Field Optical Microscopy (SNOM) [9, 10] is a powerful technique for simultaneous investigations of the morphological and optical properties of nano-structured materials. SNOM, in fact, is capable to access the nanometer spatial scales, due to its enhanced resolution with respect to conventional optical microscopy, limited by the diffraction to $\lambda/2$ (∼250 nm in the visible range). Aperture-SNOM [11] is at present the most widely employed experimental configuration. It exploits the apical aperture present at the edge of a tapered, metal-coated optical fiber either as a nanosource to illuminate the sample (illumination mode) [11], or as a nanoantenna [12] to collect the local near-field radiation scattered by the sample (collection mode). In order to detect the evanescent near-field components, the aperture is scanned at a constant distance from the sample surface (1 – 10 nm). The tip-sample distance is controlled by means of an independent feedback loop, based on shear-force detection [13–15], which simultaneously provides a direct measurement of the surface topography.

*E-mail: ruggero@fujita.kuee.kyoto-u.ac.jp; Fax: +81-75-383-2312

The possibility to control and exploit the polarization in SNOM was first pointed out by Betzig *et al.* [16]. In particular, Faraday rotation was used to image magnetic domains in magneto-optical materials [16,17]. The possibility to obtain well defined polarization states in the near-field, suggested the idea to probe the dichroic and birefringence properties of nano-structured samples by means of the so-called Polarization Modulated SNOM (PM-SNOM). In such configuration a modulated near-field polarization state, changing as a function of time, is generated at the apex of the SNOM probe, and lock-in demodulation at different harmonics is accomplished. Quantitative measurements of the local dichroism and birefringence have been demonstrated on patterned SiN membranes [18], mesoscale domains in poly(phenylene vinylene) [19] and naphthaphenylene benzidine [20] thin films, as well as on photonic block copolymers [21]. The light polarization can be modulated either by a photoelastic modulator (PEM) [18, 21–23], or by an electro-optical modulator (EOM) [19,24], or by a rotating linear polarizer [20,25]. Both illumination and collection-mode (with axial excitation [20]) PM-SNOM have been fruitfully demonstrated.

In this paper we report on the development and application of PM-SNOM techniques to test the polarization response of a DBR grating, engraved by Focussed Ion Beam (FIB) milling on a layer of GaN deposited on sapphire. We have developed a new PM-SNOM setup, working in collection-mode, with laser illumination orthogonal to the SNOM probe, specially suitable to investigate the polarization response of photonic waveguide structures. We have used a PM-SNOM approach with fixed and rotating polarizations, in both collection and transmission mode, in order to elucidate, for the first time, the local polarization properties of the DBR as a function of the incident wavelength.

II. EXPERIMENTS

The DBR sample has been etched by FIB on a 4 μm GaN layer, deposited on a 2 mm sapphire substrate. The tilt of the beam has been set to approximately 60° with respect to the normal of the substrate. The ion current used was of 50 pA. Every slab is a few tens of microns long, thus the writing process took about 5 minutes per each air-gap. This resulted in a depth of about 1.5 μm on the GaN. The distance between each slab is of about 1 μm with an air gap between them of about 250 nm.

The DBR has been tested integrated in an actual laser device [6,26]. We used a 370 nm pumping source that illuminates the laser structure and its DBR mirror through a cylindrical lens. The spontaneous emission is monitored by a monochromator and multi-channel analyzer system. We have found that, using a DBR with the geometrical configuration described above, we can reduce the threshold pumping necessary to obtain laser emission from 0.0210 MW/cm^2 (laser with facets mirrors) to 0.0134 MW/cm^2 (laser with DBR reflectors at both edges of the cavity).

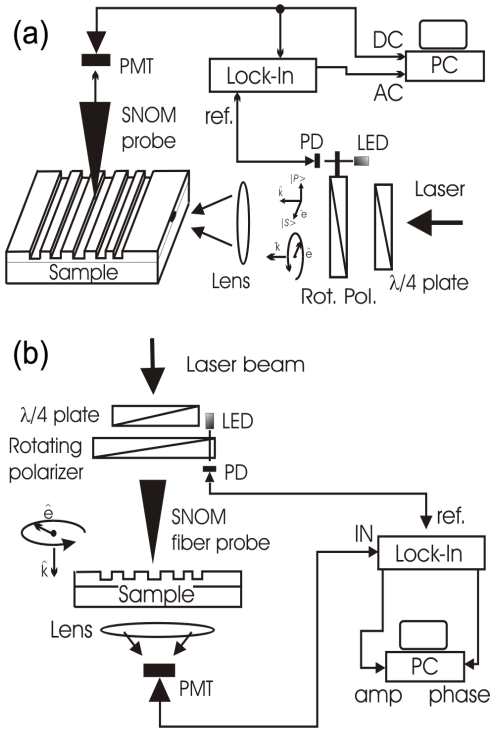

Fig. 1. (a) Collection mode SNOM setup. (b) Illumination mode SNOM setup.

The two experimental configurations, working in collection and illumination mode, are depicted in Figs. 1(a) and 1(b) respectively. In both configurations the excitation light, originated from a linearly polarized laser beam, is first passed through a $\lambda/4$ wave-plate, generating a circular polarization, and thus fed through a rotating linear polarizer. The rotary motion of the polarizer is achieved by the motor of a modified chopper device. In this way we obtain a linearly polarized laser beam with polarization angle rotating with time. A simple theoretical description of the time-modulated polarization state preparation can be achieved within the Jones-matrix formalism. Assuming a laser polarization state $P_{\rm las} = (1, 0)$, the final polarization is given by:

$$P_{\rm mod} = R^{-1}(\omega t)\cdot L\cdot R(\omega t)\cdot R^{-1}(\pi/4)\cdot C\cdot R(\pi/4)\cdot P_{\rm las} \quad (1)$$

where $C = \begin{pmatrix} 1 & 0 \\ 0 & i \end{pmatrix}$ is the matrix associated to the $\lambda/4$ wave-plate with respect to its principal axes, and $L = \begin{pmatrix} 1 & 0 \\ 0 & 0 \end{pmatrix}$ is the matrix associated to the linear polarizer. The matrices $R(\theta) = \begin{pmatrix} \cos\theta & \sin\theta \\ -\sin\theta & \cos\theta \end{pmatrix}$ take into account the fact that the principal axes of the $\lambda/4$ wave-plate are rotated by $\pi/4$ with respect to the laser in-

cident polarization, and the fact that the linear polarizer is rotating with angular frequency ω. As expected, the polarization state is given by $P_{\rm mod} = (\cos\omega t, \sin\omega t)$. We note that in our case the phase change is $\phi \propto \omega t$, differently to what occurs when using PEM in which $\phi \propto \sin(\omega t)$. Depending on the configuration, the laser light is either directly focused on the sample (collection mode) or launched into the SNOM fiber (illumination mode).

The collection mode PM-SNOM apparatus (Fig. 1(a)) has been expressly designed for the characterization of photonic structures and waveguides, in which the light must be injected and propagates parallel to the sample surface, *i.e.* orthogonally to the SNOM probe. The light beam comes either from a HeNe (632.8 nm) or HeCd (442 nm) laser and, after undergoing polarization processing, is focused perpendicularly to the DBR planes by means of a 50 mm focal length lens. The spot size is about 30 μm, *i.e.* much larger than the GaN layer. Geometrical artifacts, related to the relative motion between the sample and the focused spot, are thus negligible. To switch between *s*- and *p*- polarization in experiments at fixed polarization, we manually turn the linear polarizer (for 442 nm excitation), or use a $\lambda/2$ wave-plate (for 632.8 nm excitation) instead of the $\lambda/4$ wave-plate, removing the rotating polarizer. The scattered light is collected either through commercially available CrAl- and Gold-coated fiber probes (Nanonics Inc. and Jasco Inc.), or through tapered uncoated fibers produced by chemical etching methods [27]. A photomultiplier (PMT) is used for light detection. For polarization-modulated measurements the PMT signal is fed to a lock-in amplifier to detect the AC amplitude or phase signal, simultaneous with the optical DC signal. Modulation frequencies of the order of 100 Hz are used, so we set typical integration times of 100 ms. The sample is scanned by means of a 1 inch diameter piezo-cylinder capable of $32 \times 32 \times 8$ μm^3, or by means of a set of three smaller piezo-tubes capable of $15 \times 15 \times 6$ μm^3.

The illumination mode PM-SNOM set-up (Fig. 1(b)), fully described in previous publications [25, 28], is employed here in the transmission configuration. The excitation light is provided by two red laser diodes (emitting at 670 and 690 nm), coupled to metal coated SNOM fiber probes. The transmitted light can be collected either with a lens placed inside the piezo-scanner, or by means of a 200 μm –core optical fiber attached just underneath the sample. Light detection is accomplished by a PMT, whose signal is fed to a lock-in amplifier for PM-SNOM measurements. Simultaneous measurements of the AC amplitude and phase, together with the topography signal, are usually carried out. For experiments with fixed polarization states, the light polarization is switched before fiber launching between two orthogonal states by means of a $\lambda/2$ wave-plate, or changed randomly by twisting the SNOM fiber.

Since the aim of this experiment is to check the qualitative response of the DBR to different incident polarizations, we do not use paddles [19] or other special techniques [25] to compensate for the dichroism and birefringence induced by both the optical fiber (made of quartz) and by the aperture anisotropies [29]. We do not know exactly the polarization state of the light incident on the sample. However, we can change such a state periodically as a function of the time by modulating the polarization state of the light injected into the fiber. As a result, every local dichroic or birefringence property of the sample is evidenced in the optical maps, and specially in the AC phase image which provides a measure of the sample's dichroic axis orientation. In addition, we take advantage of the fiber's birefringence properties to change the near-field polarization state, operation accomplished by simply bending and twisting the SNOM fiber.

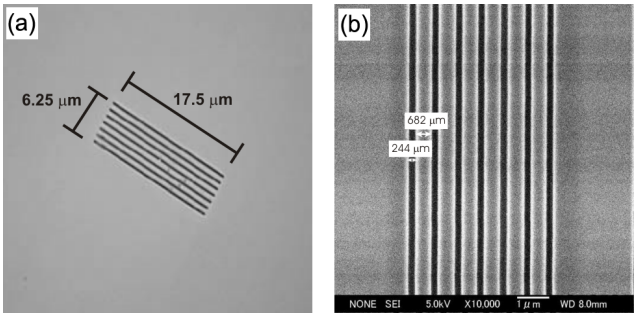

Fig. 2. Images of the DBR sample. (a) Optical microscopy and (b) Scanning Electron Microscopy.

III. RESULTS AND DISCUSSION

The DBR sample has been first imaged by means of laser scanning confocal and scanning electron microscopy (SEM), as shown in Figs. 2(a) and 2(b) respectively. We can see that the structure is constituted by six air/semiconductor periods. Each semiconductor slab is 682 nm thick and 17.5 μm long, while the width of the air gaps is 244 nm. The confocal microscope, which can perform optical profilometry measurements, confirmed an etch depth of $\sim$1.5 μm. Due to the small dimensions of the sample, it was necessary to implement our PM-SNOM apparatus with a long-working distance stereomicroscope, in order to easily target the DBR structure with the SNOM tip.

The peculiar structure of DBRs, *i.e.* the presence of alternated air/semiconductor ($n_{\rm GaN} = 2.5$) structures with a thickness comparable to the light wavelength and a length in the 10-microns scale ($>> \lambda$), makes them suitable for 2D theoretical descriptions, and for test experiments to put forward the different behavior as a function of the incident polarization.

The sample has been first characterized using the illumination-mode SNOM configuration. Fig. 3(a, b)

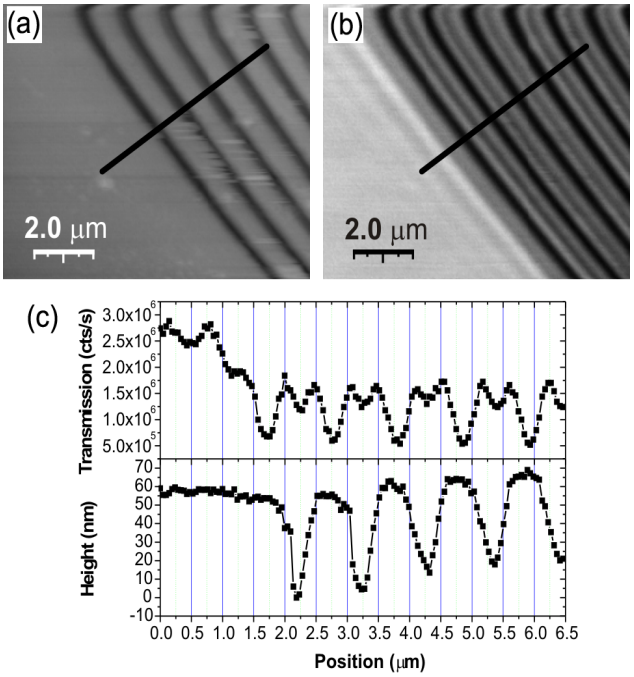

Fig. 3. DBR's topography (a) and transmission map (b) at 670 nm (10×8.1 μm^2). The light injected to the SNOM fiber was p-polarized. (c) Profiles drawn in correspondence of the black lines in (a) and (b).

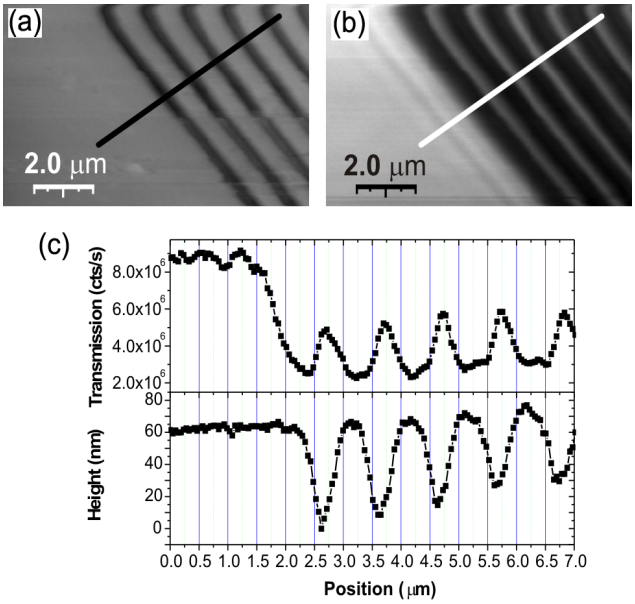

Fig. 4. DBR's topography (a) and transmission map (b) at 670 nm (10×6.1 μm^2). The light injected to the SNOM fiber was p-polarized, the fibre was twisted forming two rings. (c) Profiles drawn in correspondence of the lines in (a) and (b).

reproduce respectively the topography and the optical transmission map. Excitation is accomplished by means of a CrAl coated SNOM fiber (Nanonics Inc., 100 nm nominal aperture) at $\lambda = 670$ nm. The light injected into the optical fiber was p-polarized (vertical polarization). The fiber, single mode at 670 nm, has a length of ∼50 cm and is kept as straight as possible in order to minimize birefringence effects induced by mechanical stresses. The different spatial pattern shown by the optical map with respect to the topography, is highlighted by the line profiles in Fig. 3(c). We note the very small topography depth (∼60 nm) measured in correspondence of the air gaps, compared to the actual etch depth (1.5 μm). This is indeed due to geometrical reasons. Summing the nominal aperture's diameter to the metal coating thickness of our probes (∼100 nm), we obtain an actual probe apical diameter of the ∼200 nm. Considering that the air gap width is only 244 nm, and that our probes have cone angles of a few tens of degrees, we can estimate that the tip can not penetrate into the gaps by more than 100 nm. In particular, such a value will strongly depend on the used tip, following its actual dimensions. The V-shaped profile observed in correspondence of the air gaps (no lower plateau is observed therein) confirms our hypothesis. The optical profiles allow to make interesting observations: first of all, we see that the average transmission measured in correspondence of the DBR is attenuated by ∼50 % with respect to what detected in the unpatterned zone; secondly, the optical profile shows a double modulation pattern, in which we observe a decrease of the transmission signal in correspondence of the GaN slabs (∼50 % of the average DBR value), and a smaller modulation in correspondence of the air gaps; finally, we observe that the first modulation of the optical signal arises ∼250 nm before the topography fingerprint of the first air-gap. Subsequently, we have changed the incident polarization by twisting the optical fiber. In Figs. 4(a, b) we report respectively the topography and the transmission maps. We immediately see that the spatial pattern of the optical signal is different from what measured in Fig. 3(b). The line profiles (Fig. 4(c)) show that, again, the average transmission of the DBR structure is ∼50 % of the unpatterned zone's one. The optical profile is now somehow the negative of the topography, with a decrease of the transmitted signal in correspondence of the GaN slabs of ∼30 – 40 % with respect to the average DBR value. The slight shift (∼100 nm) between the topography and the optical signal confirm the genuine optical nature of measured signals [30,31].

The optical response of the DBR shown in Figs. 3 and 4, and in particular the strong dependence on the incident polarization, as well as the presence of modulations of the optical signal some hundreds of nm far from the topographic structures, are in qualitative agreement with what theoretically predicted by Carminati *et al.* [32] and Sandoghdar [33], for the case of single or double dielectric steps in air. The decreased transmission of the DBR is due to the elastic scattering of the slabs at an-

gles higher than those gathered by the collection optical fiber (NA ∼0.25). To evidence even further the strong dependence of the sample on the incident polarization, we show in Fig. 5 an optical transmission map in which we scan always the same line (line-scan image) changing, every 10 scans, the polarization of the near-field excitation by bending and/or twisting the SNOM fibre, as said in the previous section. Fig. 5(a) shows a 3D rendering of the optical response, evidencing different modulation patterns and shifts as a function of the incident polarization. We observe also a clear change of the average power coming out from SNOM aperture when bending the optical fiber. Light loesses, in fact, take place when the fiber is bent to form rings, in correspondence of which the total internal reflection condition is not fulfilled for all the rays propagating into the fiber. However, since the fiber is not touched during the scan of each single line, such effect does not influence the observed optical pattern, but only produces an intensity offset among the 10-lines groups. Such an offset has been easily removed during the image post-processing, by means of a line-by-line offset removal. The topography pattern (Fig. 5(b)) is also reported to assess that only a slight continuous shift takes place during the repeated scans of the same line, with no relevant implications for the optical signal.

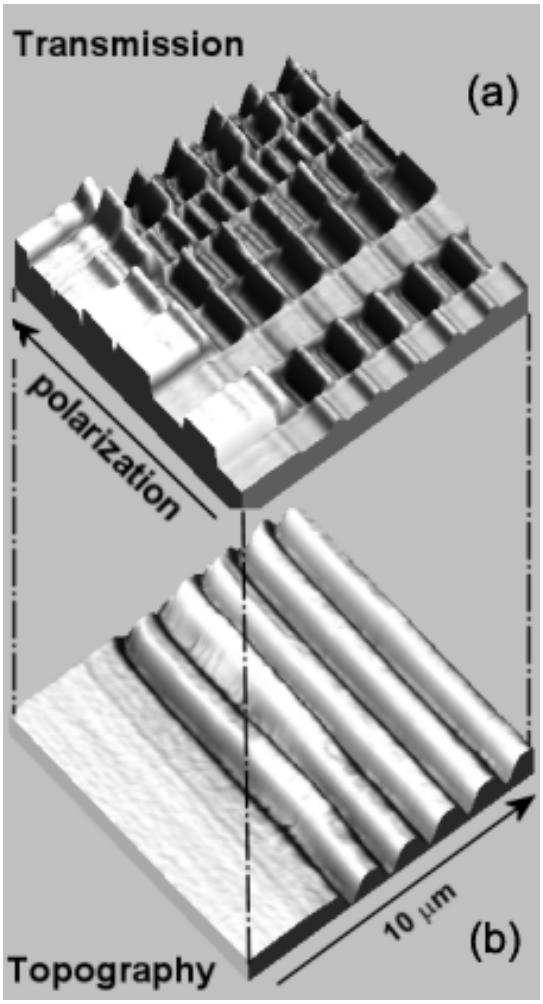

Fig. 5. 3D rendering of the optical transmission profiles (a) acquired scanning the same line (10 μm), while varying the near-field incident polarization. The corresponding topography profiles (b) show only slight changes due to mechanical and thermal drifts.

Once evidenced the sensitivity of the DBR to the polarization, we performed a test with the PM-SNOM in illumination mode. Measurements have been carried out at 690 nm with a CrAl metal coated fiber probe (Nanonics Inc., 50 nm nominal aperture). In Figs. 6(a, b) we show respectively the AC amplitude and the AC phase map. Strong modulations appear in both images, as expected. Due to the not perfect alignment among the laser beam, the rotating polarizer, and the fiber coupler, we observed that the light power coupled to the fiber was not constant, changing with the polarization angle [25]. Such effect, summed with the fiber birefringence, led to an intensity of the light coming out from the SNOM aperture modulated with time. The lock-in amplifier, thus, measured a strong signal also in the GaN unpatterned zone which, in principle, should not be sensitive to in-plane polarization variations. Fig. 6(a) shows a strong attenuation of the AC amplitude signal in correspondence of the DBR, as found previously. The phase map shows a constant value in the unpatterned zone ($\phi = -35$ deg), while sinusoidal oscillations are found in the DBR-zone ($\Delta\phi = 60$ deg). The line profiles in Fig. 6(c) highlight the different spatial patterns of the two signals.

The collection-mode SNOM is definitely the most suitable configuration to characterize the optical properties of DBRs, since the illumination geometry exactly reproduces the operation conditions in real laser devices. Investigations have been aimed to highlight the different behavior of the DBR as a function of the light wavelength and of the incident polarization. As described in sect. II, the DBR sample consists of a GaN waveguide, sandwiched between air ($n = 1$) and sapphire ($n \sim 1.77$), in which air gaps have been etched by FIB. Such waveguiding properties have been preliminarily studied by observing the DBR under an optical microscope, while changing the illumination geometry. In our setup, the focussing lens (Fig. 1(a)) can be translated by an XYZ micrometer stage. We can thus displace the light spot in order to either couple part of the light into the GaN layer (note that the spot is larger than the layer thickness), or to send the light completely into the sapphire substrate. In the first case light gets confined into the GaN layer and emerges from the waveguides only when scattered from the DBR planes. As a result the DBR appears as a bright structure on a dark background. In the second case, conversely, light is not confined and spreads all around. This makes the DBR almost indiscernible from the background at the optical microscope. The same light confinement phenomenon has been observed by SNOM. Fig. 7 shows the topography (a) and the col-

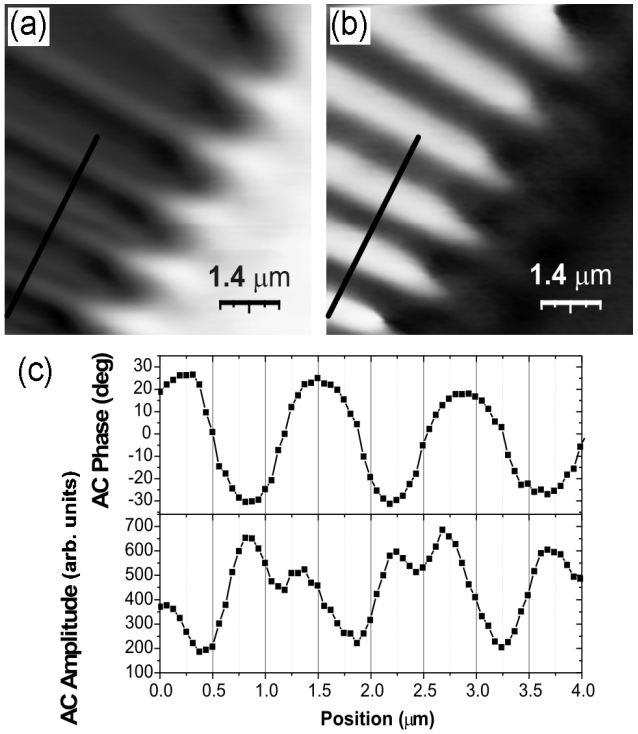

Fig. 6. AC amplitude (a) and AC phase (b) maps of the DBR acquired with the PM-SNOM in transmission-mode at 690 nm (7×7 μm^2). (c) Profiles drawn in correspondence of the lines in (a), and (b).

lection optical maps at 632.8 nm, exciting with p- (b) and s- polarized light (c). The polarization plane is here defined by the laser beam and the SNOM probe axis directions, as usual. With the help of the line profiles (Fig. 7(g)) we first observe that light emission arises in correspondence of the air-gaps; moreover, we note that the influence (interference) of the planes reflections shows up in correspondence of the fourth air gap (counting from the left). We do not observe striking differences between the two different polarizations, as in the illumination-mode measurements. Small difference are evidenced in the zoom shown in Figs. 7(d, e, f) and in the respective line profiles (Fig. 7(h), squared zones), together to a more detailed evidence of the collective DBR planes effects.

Similar measurements, carried out at 442 nm, are reported in Fig. 8, where we display the topographies (a, c) and the optical maps acquired using p- (b) and s- polarized light (d). A gold-coated SNOM probe (JASCO Inc.) was used for these measurements. Although noisy and affected by relevant scan drifts, these two maps evidence once again the DBR as a bright structure superimposed to a dark background. Moreover qualitative differences between the two polarization maps are clearly visible in the figures. To get more insight, we have exploited the newly developed PM-SNOM setup in collection-mode.

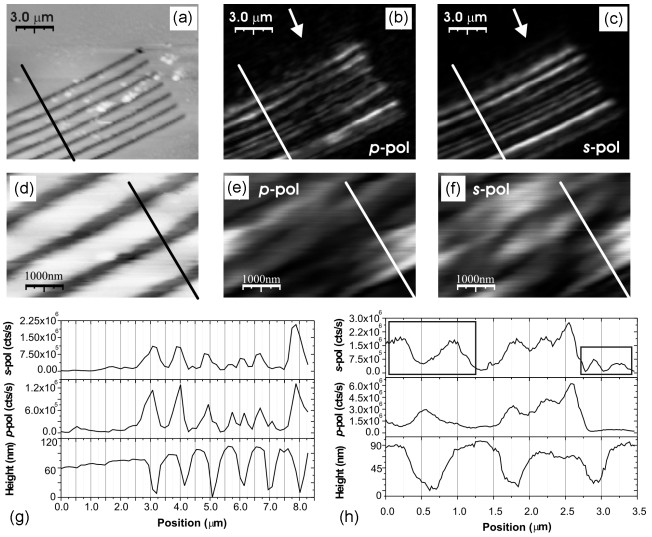

Fig. 7. Topography (a, d), and collection-mode optical maps related to (b, e) p-polarization and (c, f) s-polarization excitation at 632.8 nm. The white arrows indicate the excitation light direction. (G) Line profiles extracted from the 15 $\times$ 12 μm^2 scans (a, b, c) and (h) from the 5 $\times$ 3.5 μm^2 scans (d, e, f).

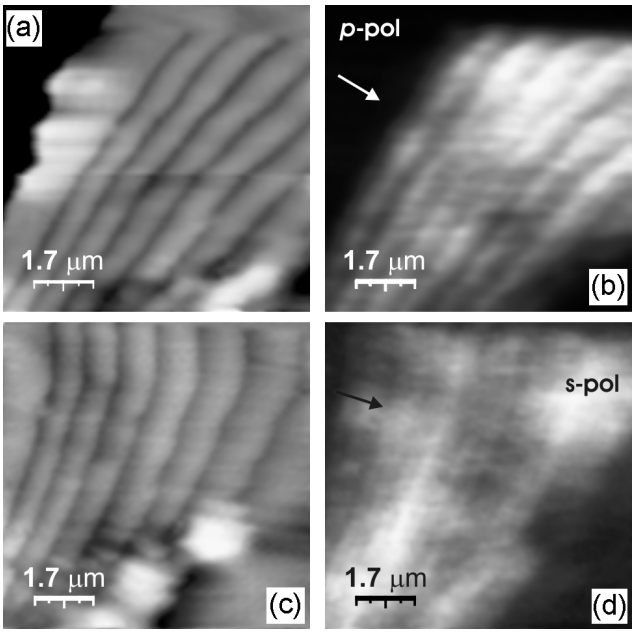

Fig. 8. Topography (a, c), and collection-mode optical maps related to (b) p-polarization and (d) s-polarization excitation at 442 nm (8.6×8.6 μm^2).

Fig. 9 shows the topography (a), the DC (b) and the AC amplitude (c) optical maps acquired on a 3.0×1.8 μm^2 area. The DC map represents the average (the integral) response of the DBR to all the incident polarizations. In particular it depends on the scattering properties of

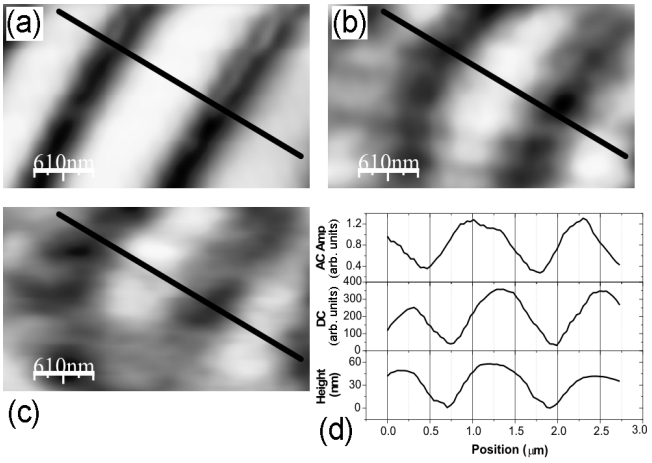

Fig. 9. Topography (a), DC optical (b) and AC amplitude maps (c) acquired with the PM-SNOM in collection-mode, exciting at 442 nm. Profiles (d) extracted in correspondence to the lines in (a), (b), and (c). Scan size 3.0 × 1.8 μm^2.

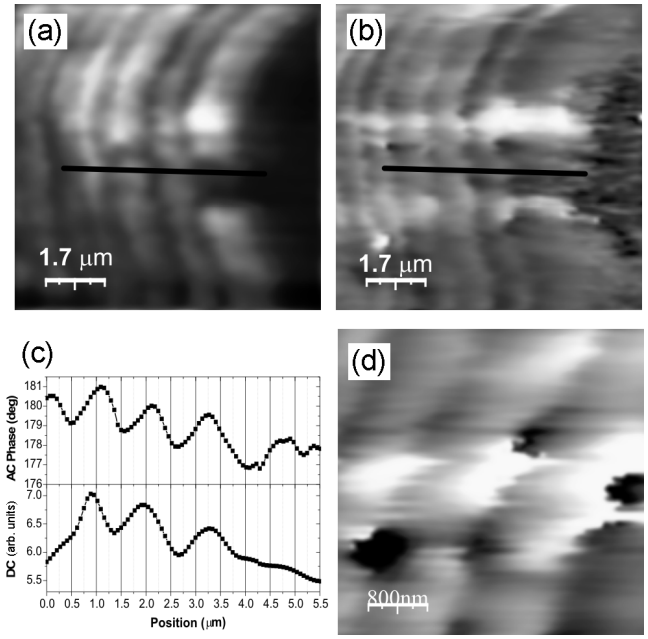

Fig. 10. DC optical (a) and AC phase maps (b, d) acquired with the PM-SNOM in collection-mode, exciting at 442 nm. Profiles (c) extracted in correspondence to the lines in (a), and (b). Scan size: (a), (b) 8.6 × 8.6 μm^2, (d) 4.0 × 4.0 μm^2.

the DBR. The comparison between the topography and the DC optical map, supported by the line profiles (Fig. 9(d)), highlight the different behavior of the DBR at 442 nm with respect to what observed at 632.8 nm (Fig. 9). Here, in fact, the zones of higher scattering correspond to the semiconductor slabs. The same behavior is observed in the measurements carried out at fixed polarizations in Fig. 8. The AC amplitude map (Fig. 9(c)), reproduces qualitatively the DC optical one, but from the line profiles in Fig. 9(d) we can note a 250 nm shift between the DC and the AC optical patterns. The polarization sensitivity of the sample is put forward by the AC phase map (Fig. 10(b)), acquired simultaneously to the DC optical map (Fig. 10(a)). With the help of the line profiles in Fig. 10(c) we can see how the phase map well reproduces the DBR features, being slightly shifted with respect to the DC map (∼150 nm). The phase fluctuations evident on the right hand side of Fig. 10(b) are due to the very low light levels detected outside the DBR planes. The sudden phase changes, corresponding to the dark areas evident in the zoom of Fig. 10(d), are simply due to 2π phase wraps. The last picture, in particular permits to assess a spatial resolution of the order of 150 nm using the 10 – 90 % criterion.

IV. CONCLUSION

In conclusion, in this report we have used the PM-SNOM working both in illumination and collection mode configuration, to carry out first measurements on DBR structures. The detection of the intensity of the local optical field gave us direct information on polarization anisotropy of the structure that is important in the design and characterization of these devices. The measurements give high resolution optical and topographical information simultaneously, allowing correlation between structural and geometrical properties of the DBR with its optical characteristics. With SNOM characterization it is possible to test the DBR structures before the actual realization of the laser.

ACKNOWLEDGMENTS

This work is carried out within the bilateral project 2A2 of the VII executive program for science and technology cooperation between Italy and Japan. P.G. acknowledges the Venture Business Laboratory for financial support. M. Alderighi is greatly acknowledged for help with early SNOM measurements and for fruitful discussions. Nanotec is acknowledged for freeware software WSxM©(www.nanotec.es).

REFERENCES

[1] R. Jambunathan and J. Singh, IEEE J. Quantum. Electron. **33**, 1180 (1997).

[2] J. Cho, S. Cho, B. J. Kim, S. Chae, C. Sone, O. Nam, J. W. Lee, Y. Park and T. J. Kim, Appl. Phys. Lett. **76**, 1489 (2000).

[3] S. Thomas and S. W. Pang, J. Vac. Sci. Technol. B **14**, 4119 (1996).
[4] E. Höfling, F. Schafer and J. P. Teithmaier, IEEE Photonics Technol. Lett. **11**, 943 (1999).
[5] C. Marinelli, M. Bordovsky, L. J. Sargent, M. Gioannini, J. M. Rorison, R. V. Penty, I. H. White, P. J. Heard, M. Benyoucef, M. Kuball, G. Hasnain, T. Tekeuchi and R. P. Schneider, Appl. Phys. Lett. **79**, 4077 (2001).
[6] T. Saitoh, M. Kumagai, H. Wang, T. Tawara, T. Nishida, T. Akasaka and N. Kobayashi, Appl. Phys. Lett. **82**, 4427 (2003).
[7] K. J. Kasunic, J. Lightwave Technol. **18**, 425 (2000).
[8] H. Wang, T. Tawara, M. Kumagai, T. Saitoh and N. Kobayashi, Jpn. J. Appl. Phys., Part II **41**, L682 (2002).
[9] D. W. Pohl, W. Denk and M. Lanz, Appl. Phys. Lett. **44**, 651 (1984).
[10] A. Lewis, M. Isaacson, A. Harootunian and A. Murray, Ultramicroscopy **13**, 227 (1984).
[11] E. Betzig, J. K. Trautman, T. D. Harris, J. S. Weiner and R. L. Kostelak, Science **251**, 1468 (1991).
[12] E. Betzig, M. Isaacson and A. Lewis, Appl. Phys. Lett. **51**, 2088 (1987).
[13] E. Betzig, P. Finn and J. S. Weiner, Appl. Phys. Lett. **60**, 2484 (1992).
[14] R. Toledo-Crow, P. C. Yang, Y. Chen and M. Vaez-Iravani, Appl. Phys. Lett. **60**, 2957 (1992).
[15] K. Karrai and R. D. Grober, Appl. Phys. Lett. **66**, 1842 (1995).
[16] E. Betzig, J. K. Trautman, J. S. Weiner, T. D. Harris and R. Wolfe, Appl. Opt. **31**, 4563 (1992).
[17] E. Betzig and J. K. Trautman, Science **257**, 189 (1992).
[18] A. L. Campillo and J. W. P. Hsu, J. Appl. Phys. **91**, 646 (2002).
[19] P.–K. Wei, Y.–F. Lin, W. Fann, Y.–Z. Lee and S.–A. Chen, Phys. Rev. B **63**, 045417 (2001).
[20] P.–K. Wei, S.–Y. Chiu and W.–L. Chang, Rev. Sci. Instrum. **73**, 2624 (2002).
[21] M. J. Fasolka, L. S. Goldner, J. Hwang, A. M. Urbas, P. DeRege, T. Swager and E. L. Thomas, Phys. Rev. Lett. **90**, 0161071 (2003)
[22] E. B. McDaniel and J. W. P. Hsu, J. Appl. Phys. **84**, 189 (1998).
[23] L. S. Goldner, M. J. Fasolka, S. Nougier, H.-P. Nguyen, G. W. Bryant, J. Hwang, K. D. Weston, K. L. Beers, A. Urbas and E. L. Thomas, Appl. Opt. **42**, 3864 (2003).
[24] T. Ha, Th. Enderle, D. S. Chemla, P. R. Selvin and S. Weiss, Phys. Rev. Lett. **77**, 3979 (1996).
[25] L. Ramoino, M. Labardi, N. Maghelli, L. Pardi, M. Allegrini and S. Patanè, Rev. Sci. Instrum. **73**, 2051 (2002).
[26] S. W. Chiou, C. P. Lee, C. K. Huang and C. W. Chen, J. Appl. Phys. **87**, 2052 (2000).
[27] S. Monobe, M. Naya, T. Saiki and M. Ohtsu, Appl. Opt. 36, 1496 (1997); R. Micheletto, N. Yoshimatsu and S. Okazaki, Opt. Commun. **188**, 11 (2000).
[28] P. G. Gucciardi, M. Labardi, S. Gennai, F. Lazzeri and M. Allegrini, Rev. Sci. Instrum. **68**, 3088 (1997).
[29] Th. Lacoste, Th. Huser, R. Prioli and H. Heinzelmann, Ultramicroscopy **71**, 333 (1998).
[30] B. Hecht, H. Bielefeldt, Y. Inouye, D. W. Pohl and L. Novotny, J. Appl. Phys. **81**, 2492 (1997).
[31] M. Labardi, P. G. Gucciardi, M. Allegrini and C. Pelosi, Appl. Phys. A **66**, S397 (1998).
[32] R. Carminati, A. Mandrazo, M. Nieto-Vesperinas and J. –J. Greffet, J. Appl. Phys. **82**, 501 (1997).
[33] V. Sandoghdar, in *Proceedings of the International School of Physics "Enrico Fermi," Course CXLIV on "Nanometer Scale Science and Technology,"* edited by M. Allegrini, N. Garcia and O. Marti (IOS Press, Amsterdam, 2001).